Commissioning MATISSE: first results

Romain G. Petrov*[a], Fatmé Allouche[a], Philippe Berio[a], Alain Chelli[a], Pierre Cruzalèbes[a], Yan Fanteï[a], Walter Jaffe[b], Andreas Glindemann[c], Stéphane Lagarde[a], Bruno Lopez[a], Alexis Matter[a], Antony Meilland[a,c] , Florentin Millour[a], Sebastien Morel[a,d], Claudia Paladini[c], Thomas Rivinius[c], Sylvie Robbe-Dubois[a], Sylvain Rousseau[a], Markus Schöller[c], Jozsef Varga[d], Gérard Zins[c]
[a]Université Côte d'Azur, Observatoire de la Côte d'Azur, CNRS, Laboratoire Lagrange, Bd de l'Observatoire, CS 34229, 06304 Nice Cedex 4, France; [b]Huygens Laboratory, Niels Bohrweg 2, NL-2333 CA Leiden, The Netherlands, [c]European Southern Observatory, Karl-Schwarzschildstr. 2 Garching 85748 Germany, [d] Konkoly Observatory, Hungarian Academy of Sciences, Konkoly Thege Miklos ut 15-17, H-1121 Budapest, Hungary.

ABSTRACT

MATISSE is the 2nd generation mid-infrared instrument designed to combine four VLTI telescopes in the L, M and N spectral bands. It's commissioning in Paranal is in progress since March 2018 and should continue until the middle of 2019. Here we report, in June 2018, the commissioning plan, tools and the preliminary results of the first two commissioning runs in MATISSE that show that the instrument is already fully operational with a sensitivity well beyond its specification. The quality of the measurements, as they obtained by the current observing procedures and delivered by the current pipeline are already good enough for a broad range of science observations. However, our results remain quite preliminary and they will be quite substantially improved by the work in progress in instrument calibration, observing procedures optimization and data processing updates.

Keywords: Astronomy, Instrumentation, Optical Interferometry, Spectro Interferometry, VLTI, MATISSE, Commissioning.

1. INTRODUCTION

MATISSE (Multiple AperTure mid-Infrared SpectroScopic Explorer) is the mid-infrared 2nd generation instrument of the VLTI[1]. MATISSE is a spectro-interferometer that combines the 4 UTs or the 4 ATs of the VLTI and analyses all interferometric measures as a function of wavelength. The data processing combines and analyzes together the interferometric and spectroscopic information to improve the angular and spectral resolution and the accuracy of color differential measures. MATISSE covers the L and M bands, from 3 to 5 μm and the N band from 8 to 13 μm, with several spectral resolutions. Its main science programs include the study of protoplanetary disks at the AU scale, the innermost dust and gas structure of AGNs, a very broad range of applications in stellar physics and some small bodies in our solar system. MATISSE is intended to be a spectro-imaging instrument with the resolution of the VLTI. We expect its extremely broad spectral coverage and the resulting enhancement of the u-v coverage to allow major breakthroughs in polychromatic interferometric imaging. MATISSE will also allow high accuracy model fits of all its spectro-interferometric measures to extract accurate quantitative parameters from the images but also to constrain the models of sources too faint or too small for imaging. A detailed description of MATISSE, its consortium and its science programs can be found in the references [2] and [3].

After more than 10 years of development and manufacturing, MATISSE has been fully integrated in the Observatory of Nice in 2016. It has passed its ESO PAE (Preliminary Acceptance Europe) in the summer 2017 and has been shipped, integrated and verified in Paranal from September 2016 to February 2017, when it has seen its first light on sky with 4 VLTI auxiliary telescopes (ATs). The laboratory performances of MATISSE and their verification until the first light on sky are described in the MATISSE AIV paper (Robbe-Dubois et al) in these proceedings[4]. This phase has demonstrated with laboratory tests that the MATISSE instrument "alone" is performing better than the contractual specifications that allow to tackle the main science objectives and is often approaching is most ambitious goals that should allow reaching the maximum VLTI performances at the MATISSE wavelength permitted by the current technology. The commissioning of MATISSE has started in March 2018 and would continue until mid 2019. It is intended to integrate and optimize the operation of MATISSE within the VLTI and verify the performances of the VLTI+MATISSE combination on sky. This

paper describes the first results of the first two commissioning runs of MATISSE. It is written very shortly after the end of the second commissioning run and presents only a provisional exploration of MATISSE performances on the VLTI. Many observations have not been fully analyzed yet and, although the data reduction pipeline already reduces correctly all MATISSE observables, we are constantly updating the reduction and calibration procedures to take into account the real behavior on the instrument as it observes targets through the earth atmosphere and the real VLTI.

In section 2 we present the key characteristics of MATISSE, its measurements, operation and data processing and the specifications that the commissioning must check. Section 3 presents an overview of the commissioning plan and schedule. Section 4 very briefly summarizes the huge work made to find calibrators for MATISSE commissioning and future science operations. Section 5 describes the operation of MATISSE with the VLTI and discusses the sensitivity limits for target and fringe acquisition. The preliminary values for the accuracy of MATISSE spectro-interferometric measurements are given in section 6 for the low spectral resolution (LR) in L and in N, and in section 7 for the high spectral resolution (HR). In the conclusion (section 8) we summarize the specifications of MATISSE that are already met, these likely to be met with some additional data processing and calibration, these that are really problematic and the points that have not been tackled yet.

2. MATISSE KEY FEATURES AND MEASUREMENTS

MATISSE is a multiaxial "all in one" instrument like AMBER. This means that the 4 input beams are merged in a common interferometric beam with non-redundant output (instrumental) baselines that allow to separate in frequency space the fringes peaks corresponding to the different input baselines set by the telescope positions projected on sky. This interferograms are spectrally dispersed to produce dispersed fringes also called x-λ interferograms that can be seen on the right screen in figure 1 that shows the MATISSE control monitor. MATISSE has two cooled spectrographs in two different cryostats. The L and M fringes are acquired by a Hawaii II detector and the N fringes by an AQUARIUS detector, both with 2048^2 pixels. The N band spectrograph has a Low Resolution (LR) mode with resolution 30 and a so called High Resolution (HR) mode with resolution 220. The L&M spectrograph has resolutions LR=30, medium resolution MR=500, high resolution HR=950 and very high resolution VHR=4500. Only the LR and MR resolutions allow observing fully L and M with a long DIT (Detector Integration Time).

Figure 1: MATISSE control monitor. On the right screen, we see 4T dispersed fringes in the x-λ interferograms. Here the upper image shows medium resolution L band fringes on the Hawaii II detector and the lower image shows N band fringes in low spectral resolution. The left screen shows the fringe detection and tracking panel (right) and the "Broker of Observing Blocs" (BOB) at the extreme left. On the fringe detection panel, we see the six fringes peaks resulting from the 2D Fourier Transform of the x-λ interferograms (L is up, N is down). The position of the fringe peak for a given baseline yields the differential OPD (the piston) on this baseline. Here the fringes peaks are close to the central horizontal line, indicating that all pistons are close to zero.

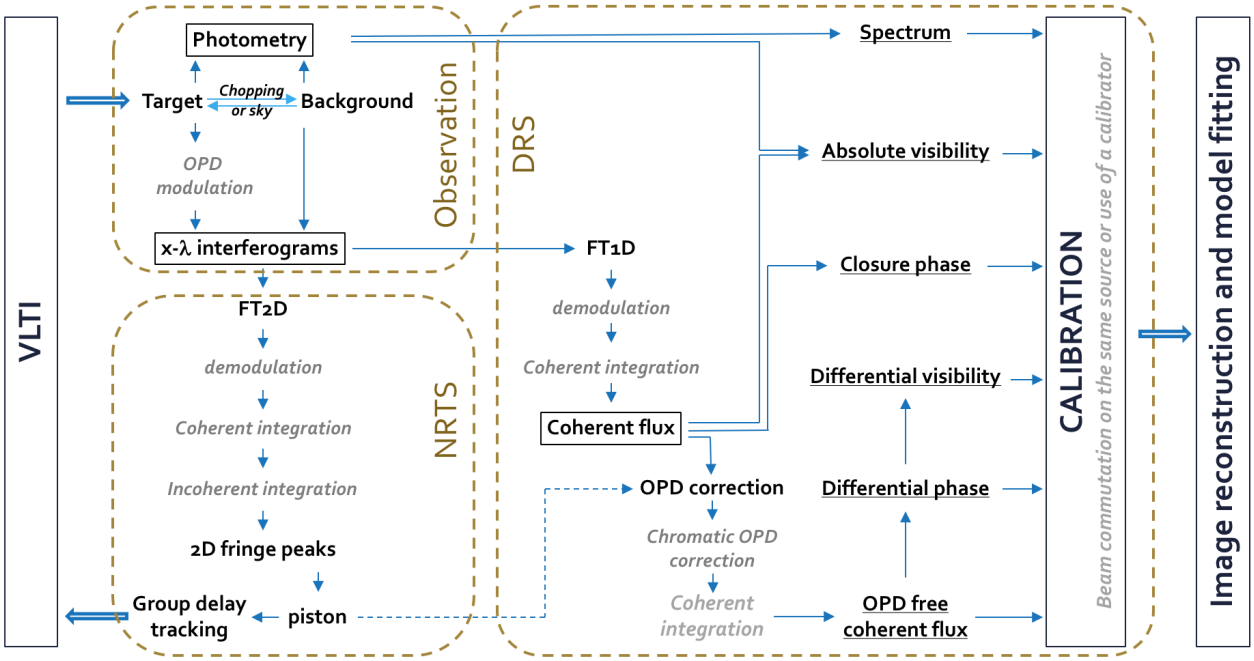

Figure 2: simplified flow chart of MATISSE data processing and measurements. The items in italic and light grey as well as the dashed paths are optional or can be different in the LM and N bands.

The figure 2 summarizes, in a quite simplified way the different steps of observation and processing that yield the MATISSE observables.

2.1 MATISSE raw data

We observe x-λ interferograms combining the 4 VLTI beams and we observe also the photometry, i.e. the flux produced by each beam.

2.1.1 Photometric measures and MATISSE observing modes

- In the HiSens (or HSE for "High Sensitivity") mode all the flux is sent to the interferometric beam (to maximize the interferometric SNR) and the photometry is measured sequentially, beam by beam, on the same pixels by closing the shutters of all beam but one.
- In the SiPhot (or SPH for Simultaneous Photometry), one third of each beam is sent to a different photometric channel that allows the interferograms and the photometry to be recorded simultaneously.

The laboratory tests in Nice and the preliminary analytical computation indicated that the SPH mode should be the best for the L band where substantial fast Strehl ratio fluctuations are expected while the N band should be observed in HSE mode. The main reason for the use of the HSE mode in N is that N band photometry mandatory needs fast chopping that will not be hardly compatible with interferometric observations using GRAVITY as a fringe tracker for MATISSE. A secondary reason is that the laboratory tests showed that the AQUARIUS detector shows an unstable spatial inhomogeneity of its non-linearity correction map that make it very difficult to deduce the correspondence between the flux measured in the photometric beam and the flux received in the interferometric beam. Thus we decided that MATISSE will be commissioned in priority in what we call the hybrid mode.

- In the Hybrid mode, we use the photometric beams in the LM cryostat (SPH hardware setup in LM) and all the flux in the interferometric beam in the N band (HSE hardware setup in N). After the interferometric observations in N, that are performed without chopping, we observe sequentially the photometric beams in N with chopping. During the photometric observation in N we still record LM fringes that are chopped.

To estimate the background, mainly in the L band, we can also use "Sky" observations that are obtained by offsetting globally the observing field for a long exposure without chopping.

2.1.2 OPD modulation

The interferometric data can also be recorded with an OPD modulation. This feature is intended to reduce the contamination of the fringe peaks from the zero-frequency peak that strongly fluctuates with the background and to reduce the crosstalk between fringe peaks. The MATISSE fringe peaks are well separated in frequency space, but the limited window used to record the interferograms and, more important, the complex and variable features in the detector gain generate a window effect (multiplicative in image space) that in frequency space produces a complex convolution pattern that extends the fringe peaks and produces crosstalk effects of a few percent. Thus, the fluctuations of the background contaminate the first fringe peaks. The crosstalk between fringe peaks also introduces errors in all measures including the closure phase. To minimize this effect, we can introduce an OPD modulation in each beam. In N band we execute typically 10 OPD steps within a N band coherence time (200 ms). The stroke of the modulation is set in order for each baseline to be modulated at a different frequency. When we demodulate one baseline, in the data processing, all other baselines and the zero-frequency peak are modulated to have a zero-average value. The laboratory tests have shown that in N band the modulation very substantially improves the quality of all measurements. We therefore decided to use systematically a ten steps modulation in the N band, with 20 ms individual frames and a coherence time of the order of 200 ms. After demodulation, the 10 frames are coherently integrated within a coherence time. This requires a careful calibration of the OPD modulation, that has been performed and extensively tested in Nice and a good synchronization between the modulation and the detector readout that represented a substantial fraction of the commissioning tests at Paranal.
In L band the detector is too slow and the coherence time too short to allow reading more than one frame per coherence time. Thus, we cannot modulate over several frames in the coherence time. We still expect that a modulation cycle longer than the coherence time, without coherent addition of the demodulated frames, will improve the quality of the data by cancelling some mid-term instrumental effects (i.e. slower than the turbulence but faster than the calibration cycle) as indicated by the laboratory tests. However, during the first commissioning runs, we tested that the modulation in L is operational but we never used it to record data.

2.2 MATISSE target acquisition

The goal of the target acquisition is to make sure that the source is well centered on the MATISSE image plane spatial filter or slit. The automatic alignment procedure of MATISSE, on its internal source, sets the so-called "MATISSE reference pixels" that are the positions of the center of the spatial filter images on the MATISSE detectors. This alignment is performed every day but has proven to be stable at least on a week scale.

To acquire a target, we set MATISSE in a non-dispersed mode, without spatial filters, and we use the photometric beams to obtain images on the target on the detector. Then, the Near Real Time Software (NRTS) computes the difference in position between the center of the target and the MATISSE reference pixels and moves the telescopes to set the L band images in the right place. To do this, it actually updates the reference position for "laboratory guiding" on the IRIS VLTI subsystem. Then, IRIS tracks the target on this updated reference pixels, which assumes that the target is bright enough in the K band. If the target is not bright enough in the K band, we can directly drive the telescopes from MATISSE, in L band for N band observations or in N band for L band observations.

The transverse atmospheric chromatic dispersion (TADC) is corrected in IRIS between K and L, by updating offsets on the IRIS reference pixels, and by MATISSE between L and N, by moving internal periscopes.

2.3 MATISSE fringe acquisition

To detect the fringes, the NRTS performs 2D Fourier Transforms of the x-λ images, that are " re-sampled" to have a constant fringe spacing constant steps in wavenumber $\sigma=1/\lambda$. Then, if the OPD for a given baseline is within the coherence length, the averaged modulus of the 2D FT shows a fringe peak at a position corresponding to the residual OPD (or "piston"). In the fringe search procedure, we scan the VLTI delay lines to find all fringe peaks. Then we use the fringe peak positions to compute the residual piston that is sent to the VLTI delay line to perform a "group delay tracking".

The limiting sensitivity for the observation of MATISSE is therefore set by the possibility to detect the fringe peaks. To maximize this sensitivity the fringe peaks are integrated coherently (after demodulation if a modulation has been used) within a coherence time and incoherently within the typical fringe drift time, that strongly depends from the quality of the VLTI delay line model. Typically, we use up to 10 s for the incoherent integration. The maximum incoherent integration time is set by the length of the observing exposure, that is of the order of 1 mn to allow a good calibration cycle and to avoid producing oversized raw data files.

2.4 MATISSE measurements and data processing

The data reduction is summarized in figure 2. This is a very simplified flow chart of the Data Reduction Software (DRS) that hides many "small" cosmetic and bias corrections and hides the fact that some procedures might be iterative.

Each frame is corrected for detector biases, ADU-photon conversion, non-linearity, bad pixels and distorsion. This phase, called "detector cosmetics" is based on daytime calibration.

The photometric signal is corrected from the background by a subtraction of the "sky flux" that has been obtained either from a sky exposure obtained by offsetting the telescopes (in L and to correct interferometric beams) or from chopping with a mirror in the telescope train (M2 with UTs, M6 with ATs).

Then the "target" signal in the photometric channels is used to compute the source spectrum.

In each spectral channel, a 1 D Fourier Transforms produces the fringes peaks that give the coherent flux (visibility x flux). The coherent flux is integrated within the coherence time (typically 10 frames in N and 1 frame in L) after demodulation if the data has been obtained with modulation, which is always the case in N and never so far in L.

The modulus of the average coherent flux is combined with the source photometry to obtain the raw target visibility.

The average coherent directly yields the closure phase that is the argument of the bi-spectrum of baseline triplets.

The average coherent flux in all spectral channel is used to compute the residual piston, combined with a model of the chromatic OPD. This allows to add coherently the coherent flux in all spectral channels to obtain a reference channel. Then the cross-spectrum between the coherent flux in this reference channel and the coherent flux in each spectral channel yields the differential phase (the phase of the cross-spectrum) and the differential visibility (modulus of the ratio between the cross spectrum and the squared modulus of the coherent flux in each channel).

2.5 Calibration of MATISSE measurements

The spectrum is calibrated using spectral calibrator that yields the spectral response of MATISSE.

The raw average visibility is affected by an "instrument + atmosphere" instrumental visibility. It is calibrated using a calibrator, i.e. a star with known visibility. The MATISSE specification is to be able to execute a calibrator-science cycle in one hour.

The closure phase is in principle a self-calibrated measure. In practice, it is sensitive to instrumental features that introduce crosstalk between the beams (the optics have been carefully designed to reduce this effect but are unlikely to cancel it completely) and between the baselines, mainly due to the window effected enhanced by the variable features in the detector response. Thus, for very high closure phase accuracy, we can use the "Beam Commutation Device" (BCD) of MATISSE that switches the input beams 1&2 and 3&4. That changes the sign of the closure phase seen by the instrument without changing the instrumental contributions to the closure phase. For a full calibration of the closure phase, we need to observe the 4 input sequences "1234"; "2134"; "2143" and "1243". The closure phase can also be calibrated using a calibrator with zero closure phase. The BCD calibration cycle can be executed within minutes, on the science target itself while the time delay between the source and a calibrator is typically 30 mn.

The differential visibility and the differential phase need a good correction of the longitudinal chromatic OPD for high accuracy measurements. They can also be calibrated from the known differential measures in some spectral channels. This is particularly applicable for high spectral resolution measures around a spectral line where the differential measures can be fitted in the nearby continuum. They can also be calibrated on a calibrator.

The BCD inverts the source differential phase for baselines b1 and b2 and can therefore be used for high accuracy differential phase measurements in low spectral resolution.

2.6 MATISSE key specifications

Table 1 summarizes the key specifications that must be checked during the commissioning. The "technical specifications" are the ones agreed with ESO in the contract of the consortium MATISSE. They ensure that MATISSE can achieve its minimum science objectives. The "goals" are the value that the consortium wished to achieve at the beginning of the project, for the maximum science objectives that the VLTI and MATISSE could tackle. The performances "expected by design" were updated during the design phase and the last column gives an update of the performances from laboratory

measurements of the MATISSE instrument alone[4]. The "sensitivity estimates" are for a coherent flux SNR=3 within a coherence time (75 ms in L and 200 ms in N). The accuracy specifications in N are for a 20 Jy point source.

Name	Tech Specs specific.	Tech Specs Goal	Expected by design	Updated from lab. for the instrument alone
Sensitivity in L UT (4T, LR)	≤ 0.75 Jy	≤ 0.15Jy	Needs Tr ≥ 15%	Estimated Tr ≥ 29%
Sensitivity in L AT (4T, LR)	≤ 7.5 Jy	≤ 1.5Jy		
Sensitivity in N UT (4T, LR)	≤ 4 Jy	≤ 1 Jy	Needs Tr ≥ 15%	Estimated Tr ≥ 12%
Sensitivity in N AT (4T, LR)	≤ 60 Jy	≤ 12.5Jy		
Visibility accuracy L UT	≤ 7.5%	≤ 2.5%	≤ 0.6%	≤ 0.5%
Visibility accuracy L AT	≤ 7.5%	≤ 2.5%		
Visibility accuracy N UT	≤ 7.5%	≤ 2.5%	≤ 0.7%	≤ 2.6%
Visibility accuracy N AT	≤ 30%	≤ 10%		
Diff. phase accuracy L UT	≤ 30 mrad	1mrad	≤ 11mrad	≤ 6.6 mrad
Diff. phase accuracy L AT	≤ 60 mrad			
Diff. phase accuracy N UT	≤ 30 mrad	1mrad	≤ 11mrad	≤ 4.4 mrad
Diff. phase accuracy N AT	≤ 60 mrad			
Closure phase accuracy L UT	≤ 40 mrad	1mrad	≤ 8mrad	≤ 5.2 mrad
Closure phase accuracy L AT	≤ 80 mrad			
Closure phase accuracy N UT	≤ 40 mrad	1mrad	≤ 8mrad	≤ 5.8 mrad
Closure phase accuracy N AT	≤ 80 mrad			
Diff visibility accuracy L UT	≤ 1.5%	≤ 0.5%	≤ 0.2%	≤1.4 %
Diff visibility accuracy N UT	≤ 3%	≤ 1%		≤0.9 %
Diff visibility accuracy L AT	≤ 5%	≤ 2%	≤ 0.5%	≤1.4 %
Diff visibility accuracy N AT	≤ 30%	≤ 10%		≤0.9 %

Table 1: main MATISSE specifications that must be checked during the commissioning. The columns signification is in the text

3. MATISSE COMMISSIONING PLAN

3.1 The commissioning runs

The commissioning plan of MATISSE has been divided in several commissioning runs. The initial plan proposed by the consortium at the PAE has been updated to adapt to the availabilities of the VLTI. Here we summarize the goal and updated schedule of the runs. We also give the main results of the runs already executed, before detailing the estimated MATISSE/VLTI performances in the next chapters.

3.2 Operations (run "AIV-sky" or "1_O", March 2018)

In spite of its name this is the first commissioning run. Its main goals are:

- To commission the operation of MATISSE in the VLTI environment.

This has been fully achieved, from the operation of MATISSE with the standard VLTI instrument OS environment, using a Broker of Observing Blocks (BOB) in which we fetch OB prepared with the Visitor Observing Tool (VOT). MATISSE is ready to be operated has any VLT instrument.

- To make a first set of sensitivity estimates.

This is detailed in the next chapter, indicating that MATISSE is performing better than its goals and therefore much better than its contractual specifications

- To test the MATISSE pipeline.

MATISSE pipeline was usable almost from the beginning of the first commissioning run, but we detected a lot of software bugs and many needs to adapt the data reduction to the actual behavior of the instrument on the VLTI. This is discussed for each measurement presented above.

3.3 Measurement accuracy in LR L&M (Run 1_A, May 2018)

The initial goal of the run was to evaluate the performance of the LR observing modes in L and in N, in order to report to ESO early enough (June 2018) to allow considering offering MATISSE in LR on the VLTI in the September 2018 "Call for Proposal" for the ESO observing period P103.

This run allowed to implement and to validate many Operating System, NRTS and DRS corrections.

The NRTS is now able to process all frames, while in March it was too slow to process more than one out of 4 to 5 frames. This allows to actually add coherently typically 10 frames in N and improves the fringe detection sensitivity.

The overheads have been quite substantially reduced and now a typical observation, with 4 interferometric exposures and 8 photometric exposures in N (and therefore 12 interferometric exposures in L) takes 20 mn, for 12 mn open shutter time.

Changing the spectral resolution of the instrument can be done in less than 2 mn and does not require repeating instrument calibration. We therefore decided to combine LR and HR (or MR) observation after the acquisition of the target and of the fringes. Therefore, we could make a preliminary evaluation of the HR mode performances during this run.

3.4 Run 1_B (July and September 2018): Higher spectral resolutions and M band

We have to update the sensitivity limits, mainly with UTs because we had only 2 half nights with 4UTs so far, that were dedicated in priority to an evaluation of the measurement accuracy.

This run will also be dedicated to a more detailed study of the higher spectral resolutions, HR in N and MR and HR in L.

It will also investigate the performances in the M band.

3.5 Run 1_C (December 2018): imaging with all ATs configuration and NAOMI performance update

The first runs have been executed with a fixed AT configuration. The run 1_C will test imaging with 5 AT configuration, with a relocation of 2 ATs every two days.

As the ATs will be equipped with Adaptive Optics Systems (called "NAOMI") by November 2018, this run will also be used for an update of the performances of MATISSE with AO. Currently the performances have been evaluated only with the tip-tilt correction of the ATs. NAOMI will have an important impact in the K band (IRIS tracking capability) and a significant improvement in the L band for median seeing conditions.

3.6 Run 1_D: GRA4MAT: operation of MATISSE with GRAVITY as an external fringe tracker (>April 2018)

To achieve its full potential, in particular in the higher spectral resolution modes in the L and M bands, MATISSE needs an external fringe tracker. The internal fringe tracker of GRAVITY, that operates in the K band, will be used for that. The selected option is to use GRAVITY "as it is" without any modification and to use its signals to drive the VLTI delay lines instead of internal GRAVITY delay lines. This will reduce the performances in K, for GRAVITY itself because the bandpass of the VLTI actuators is lower, but should be good enough for the less demanding L and N band MATISSE observations. This run requires Operating System modifications to allow the two instruments to work together. Because of manpower limitations, the commissioning of MATISSE with GRA4MAT cannot be earlier than April 2019.

4. TARGETS FOR THE COMMISSIONING OF MATISSE

For the commissioning of MATISSE and for its future operation, we had to find calibrators usable in the L and N bands, where there are relatively little accurate flux and angular size measurements. One of us (Pierre Cruzalèbes) developed a combination of all existing information to produce the MATISSE Stellar Diameter and Flux Catalogue. The original aim is to provide information on the angular diameter and flux in the L, M, and N spectral bands for as many stars as possible, and identify the potential calibrators among them.

To reach these goals, we use as first input catalogue the JMMC Stellar Diameter Catalogue (JSDC, 465 605 sources), completed with the diameter values of the JMMC Measured Diameter Catalogue (JMDC, 785 sources), and those of the MIDI list of Calibrator Candidates (403 sources). Thus, our catalogue contains 465 838 different targets, gathering measurements and estimations (mainly from the surface brightness method; see Chelli et al. 2016[5]) of the angular diameter.

We compile the flux density measurements taken from a set of infrared photometric catalogue (WISE+ALLWISE, AKARI, COBE/DIRBE, GLIMPSE, MSX6C, IRAS/PSC+FSC, JP11, and 10mu-Catalogue). We complete the flux measurements

with the flux estimates in the MIR-spectral bands given the Cohen list of spectrophotometric standards (435 entries), and by the blackbody fluxes computed thanks to the effective temperature and the angular diameter estimates given by the MIDI catalogue and the brand-new Gaia-DR2 survey. Thus, our catalogue gathers 7 flux values in L (3.2 to 3.9 µm), 8 in M (4.5 to 5 µm), and 12 in N (8 to 13 µm). Because of the high dispersion of the flux values noted in each spectral band, we give the median value, and compute the median absolute deviation, which gives a rather robust estimate of the statistical dispersion of the flux values.

Finally, we identify the potential calibrators identified thanks to the 6 following criteria:

1. reliable angular diameter estimate given by the JSDC;

2. single star or known binary in the Washington Double Star Catalogue with angular separation greater than 1";

3. favorable SIMBAD object type, i.e. avoiding possible binaries or pulsating stars;

4. no infrared excess identified with the K-[22] color excess (Wu et al. 2013, ApJS 208), and with the MIR excess statistics reported for the Tycho-Gaia stars (McDonald et al. 2017, MNRAS 471);

5. no infrared extent reported by the WISE/ALLWISE and the AKARI surveys;

6. no MIR variability reported by the WISE/ALLWISE survey.

The first 3 criteria are already included in the JSDC catalogue. We add the last 3 criteria more specific to the MIR spectral range. We find that 222 081 stars of our catalogue fulfil these 6 criteria simultaneously. Thus, 48% of the total number of the entries of our catalogue can be considered as potential calibrators.

The MATISSE Stellar Diameter and Flux Compilation Catalogue can be uploaded from the "Commissioning" section of the MATISSE Twiky https://matisse.oca.eu/foswiki/bin/view/Commissioning/WebHome.

5. SENSITIVITY LIMITS FOR MATISSE ACQUISITION

5.1 Target acquisition

Figure 3 shows the SNR for target acquisition with MATISSE as a function of the estimated source flux in the L band in Jy. This SNR has been computed from an analysis of the acquisition images. It represents the average height of the source signal divided by the rms of the noise outside the source, after filtering to keep only the structures that have the typical size of the Airy disk. As the acquisition images are used to compute the photocenter of the image and correct its position, a typical SNR of 5 to 10 is necessary for a reliable photocenter estimate. The extrapolation of the fit of the function SNR=f(flux) yields image acquisition limits of the order of 2 or 3 Jy in L with the ATs and between 0.1 and 0.3 Jy in L with the UTs. We lacked time to fully test the N band acquisition limit but we found that L band acquisition was systematically easier even for the very red Circinus Galaxy. For all sources other than the Circinus Galaxy, we actually found that the best way to acquire the target was to use IRIS in the K band. The case of extremely red sources still has to be evaluated.

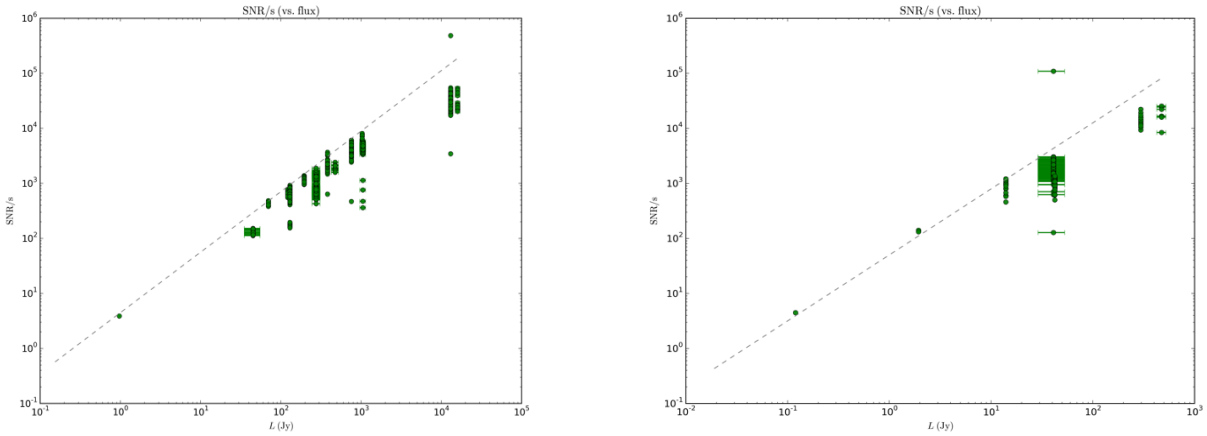

Figure 3: SNR of the acquisition image in L band as a function of flux for the ATs (left) and UTs (right). This can be extrapolated to provisional acquisition limits of about 2-3 Jy with ATs and 0.1-0.3 Jy with UTs

5.2 Fringe acquisition limits

In L band with ATs, we successfully detected and tracked fringes on HD90295, which has a flux in Jy of 0.2±0.1. In N band with UTs, we followed fringes on HD122156, which has a flux in N of 0.21±0.02 Jy. In both cases we had an excellent seeing, of the order of 0.6 arcsec, but the NRTS was not fully optimized for this observations in March, as we were not able to process all frames. This "record" numbers are supported by the extrapolation of the SNR of coherent flux as a function of source flux. They both are better than the goals, of MATISSE given in table 1. For the N band, we did not try to make "record" fringe acquisition with the ATs, but the extrapolation of the plot SNR(coherent flux)=f(flux) in figure 4 yields an SNR=5 in 10 s for a 10 Jy source that we consider as a reasonable detection and tracking limit. The exact fringe tracking limits will be evaluated again in July.

6. ACCURACY OF MATISSE LR MEASUREMENTS

6.1 SNR of the coherent flux in N band

The figure 4 shows the SNR of the coherent flux as a function of flux for all targets observed in May. The 20 ms frames were coherently averaged over 200 ms after demodulation and incoherently averaged over one full 46 ms (open shutter) exposure. The plot for the ATs shows the expected variation as a function of flux and yields the 10 Jy fringe tracking limit discussed above. The plot for UTs shows the expected SNR gain for faint targets, with an SNR of the order of 100 with UTs instead of 5 with ATs for a 8 Jy target, but the SNR with UTs seems to saturate around 100. As we note that we also do not observe any SNR higher than 200 with ATs, we might have an upper limit for this SNT that needs to be investigated. In July, we will have to explore fainter targets with UTs, to see if the UT SNR behaves in parallel to the AT one for targets between 0.2 and 2 Jy.

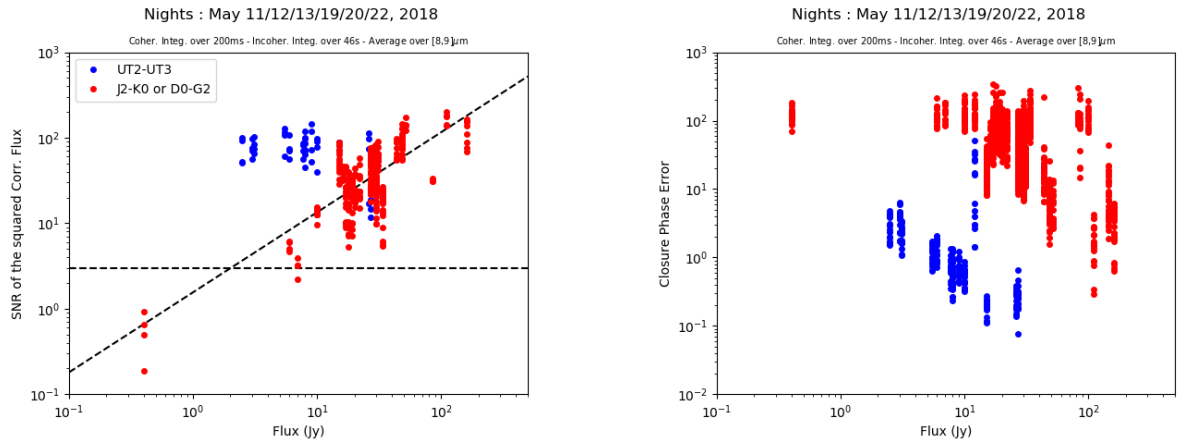

Figure 4: SNR of the coherent flux (left) and on the closure phase (right), for each 46 s exposure, in N band between 8 and 9 µm, as a function of the catalogue flux in N in Jy. The red dots are for ATs and the blue dots for UTs.

6.2 SNR on the closure phase in N band

The figure 4 also shows the closure phase error in degrees, in LR N band averaged between 8 and 9 µm. The saturation of the error for faint sources with the ATs corresponds to a closure phase nearly distributed between ±π. With ATs, the closure phase accuracy for a 20 Jy source seems distributed between 10° and 100°, which is far from the 5° specification. For the same flux, the average coherent flux SNR is of the order of 20, that corresponds to a closure phase error of 60 mrad or 3.5°. This discrepancy might mean that the instantaneous coherent flux fluctuates substantially and further degrades the closure phase accuracy. On the other hand, on H Sco (N=30±7 Jy) we have a closure phase accuracy well below 10° *per spectral channel* between 8.2 and 8.8 µm computed from repeated observations of this target with the ATs, as indicated by figure 5. On a poor night, the closure phase accuracy can be multiplied by more than 5 on the same source. This point clearly needs further investigation. With UTs this 5° accuracy is achieved for sources fainter than 3 Jy and it seems possible to go quite fainter than 0.3° accuracy for sources brighter than 20 Jy. However, this plot describes only the rms of the closure phase over time and might neglect instrumental biases.

When we compare the coherent flux and the closure phase plots in figure 4, we see that the UTs closure phase SNR improves with the source flux while the coherent flux SNR saturates. This might indicate that the limit on the coherent flux SNR is due to something that does not affect the closure phase, like the piston jitter over the coherent time.

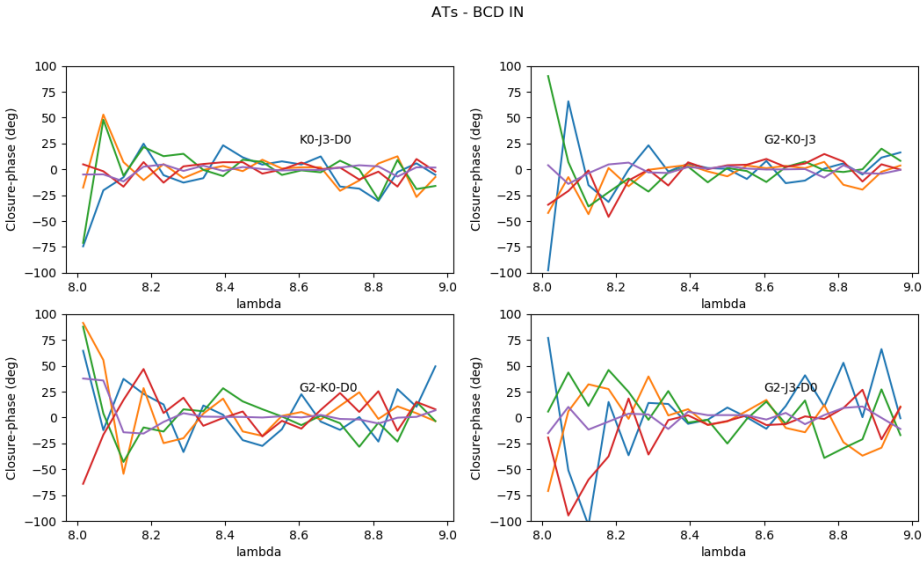

Figure 5: Closure phase obtained on the calibrator H Sco (N=30±7 Jy) observed several times over 2 good nights.

6.3 Closure phase in the L and N bands for a well resolved binary

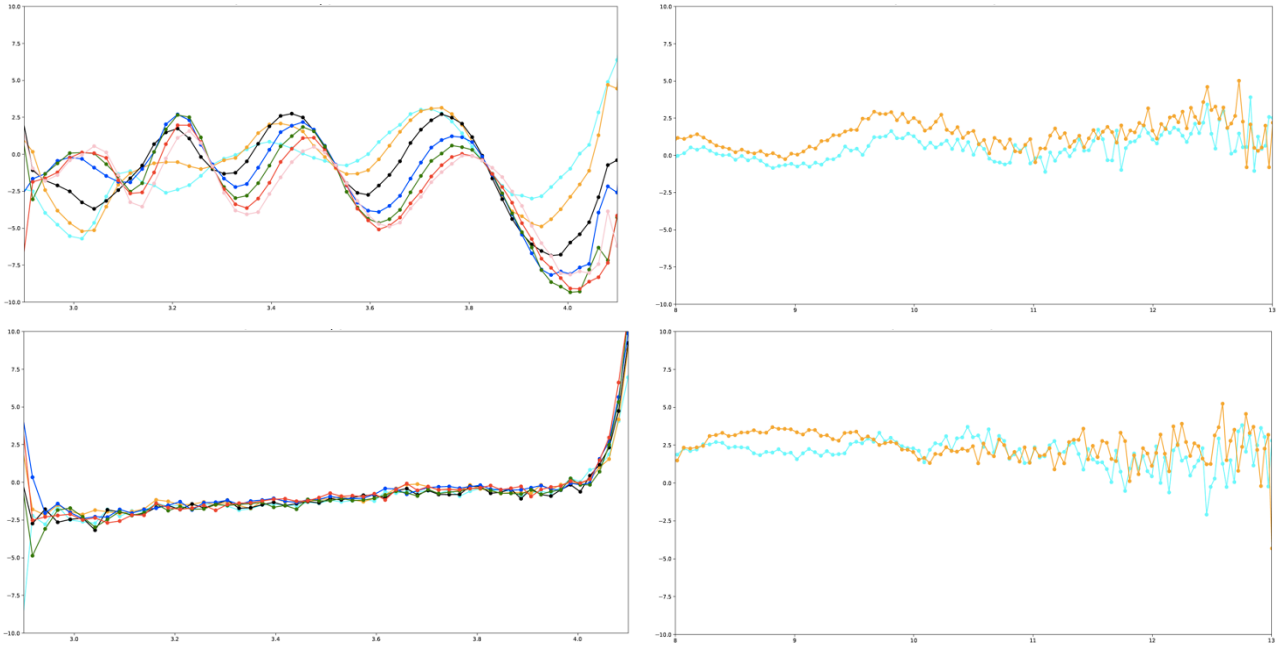

Figure 6: Closure phase in LR L (left) and N (right) with UTs obtained on a well resolved binary (up), with a separation of the order of 125 mas, and on calibrators (down) and estimated magnitudes 30 Jy in L and 15 Jy in N. The AT triplet was on A0-K0-J0. The UTs were UT1-UT2-UT4. The L band magnitude of the calibrator HD171094 was estimated by MATISSE ~100 Jy (80±50 Jy in the catalogues). The magnitude of the N band calibrator HD is estimated ~24 Jy. The exposures are distributed over 10 mn in L band and 3 mn in N band.

Figure 6 shows the closure phase as a function of wavelength obtained on a well resolved binary (125 mas separation while the resolution on the largest baseline is 5 mas in L and 15 mas in N). We see the closure phase oscillations typical for a resolved binary. In L band the closure phase accuracy on the 100 Jy calibrator is less than 0.3° per spectral channel (rms over time) but we see an instrumental closure phase linear variation of up to 2° from 3 to 4 microns and a strong contamination of the closure phase by chromatic OPD after 4 microns. In N band with UTs (24 Jy calibrator) the error per spectral channel (differential closure phase) goes from 0.5° at 8 µm to 1.5° at 12 µm but we see global instrumental changes larger than 1.5° in a few minutes between 8 and 10 µm. This indicates that the closure phase, that is in principle a absolute measurements needs to be calibrated and corrected from residual piston and chromatic OPD contaminations.

6.4 Absolute visibility accuracy in L band with ATs

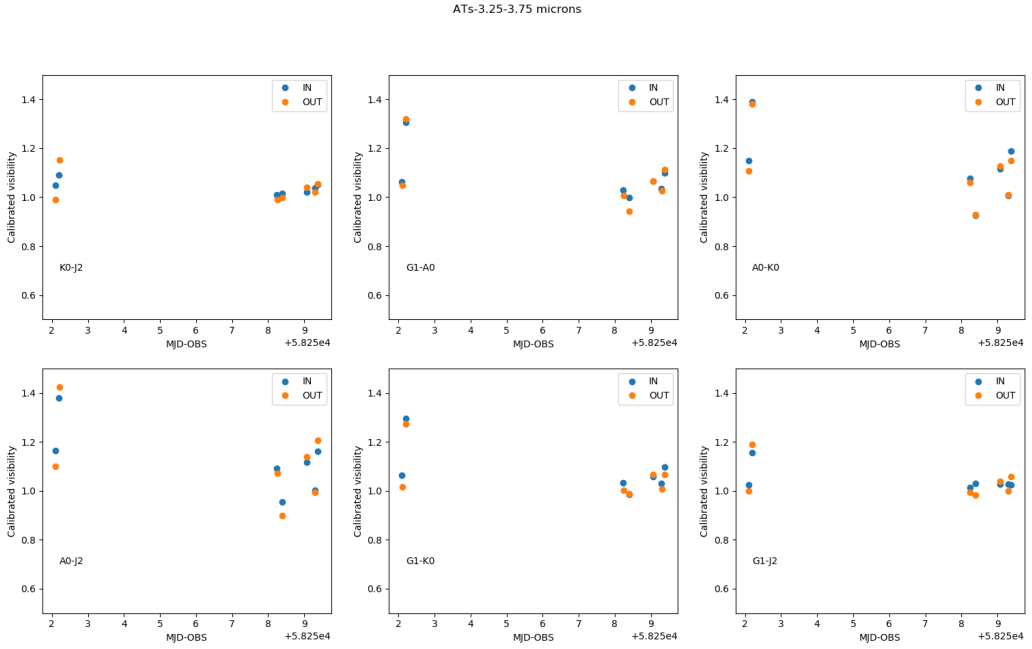

Figure 7: Stability of the calibrated visibility in L band with ATs. Each figure is for the baseline indicated in the figure. The shortest baselines are K0-J2 (49 m) and G1-J2 (58 m) and the longest are A0-K0 (128 m) and A0-J2 (129 m). Each point represents a calibrated visibility from a triplet of calibrators. The blue and orange dots are respectively for the "BCD in" and "BCD out" configurations. Each calibrator has been corrected from its diameter estimated from JSDC. We used data from three nights: May 13, with a seeing>1.2 arcsec (the dots on the left part) and May 18 and 19 with a seeing<0.7 arcsec. The dispersion of measures increases with the seeing and with the baseline.

The relevant absolute visibility accuracy is the stability of the calibrated measures in a Cal-Sci-Cal sequence where the science target is calibrated by the average of two calibrators observed just before and just after. To test this accuracy, we have observed a large number of calibrator triplets, and made statistics on the calibrated absolute visibility. Our triplets have been selected to be reliable calibrators brighter than 15 Jy in N. All these stars are brighter than 100 Jy in L and we are really testing the stability of the instrumental visibility here and not the fundamental noise limits. Some results in the L band are displayed in the figure 7 that plots the calibrated visibility as a function of the Julian date, for each baseline. The raw visibility on each calibrator has been corrected using the JSDC estimation of its angular diameter. The plots represent three nights. On May 13, we had a poor seeing, always larger than 1.2 arcsec and on May 18 and 19 we had a much better seeing almost always smaller than 0.7 arcsec. We see that the dispersion of measures strongly increases with the seeing, for all baselines and with the baseline, even for the good seeing. The difference in behavior between the shortest baselines K0-J2 (49 m) and G1-J2 (58 m) and the longest baselines A0-K0 (128 m) and A0-J2 (129 m) indicate that we are sensitive to errors in the diameter estimates.

The overall dispersion of the measures for all baselines are 8% rms. However, if we consider only the two good nights we have a rms=0.6% for the shortest baseline (K0-J2) and a rms=9% for the longest baseline (A0-J2). We estimate that with an appropriate correction of the diameters we can have an accuracy of the order of 1% for good seeing.

The difference between the results in good and bad seeing confirm the sensitivity of L band measures to the speed of the piston jitter, that was identified as the main cause for uncertainty on the L band absolute visibility. All the observations were made with a frame DIT=75 ms, that allows to cover the 3-4 µm window in LR_L with the Hawaii detector in its slow read mode that yields the best SNR. A shorter DIT would give absolute visibilities much less sensitive to seeing changes but would imply reducing the spectral window. Repeated observations of the same target (H Sco) in different conditions have confirmed the sensitivity of the L band measures to seeing changes as they show a clear correlation between the measured visibility and the atmospheric coherence time τ_0.

6.5 Accuracy of the calibrated closure phase in L band with ATs

We have used the same triplets of targets for a Cal-Sci-Cal calibration of the closure phase. The selection of triplets has not been optimized for closure phase calibration has they have been selected to be close in time rather than close in chromatic OPD. The results are summarized in figure 8 that shows that the dispersion of calibrated closure phases is almost insensitive to seeing and baseline. The overall rms for the closure phases of these bright (>100 Jy) targets, calibrated like the absolute visibility by sources close in time is ≤0.8° for all baseline triplets. This 14 mrad value is better than specifications, far from the goal (1 mrad) and larger than the MATISSE only contribution of 5 mrad. The calibration of the closure phase with the BCD and using the chromatic OPD estimates from the differential phase is a work in progress that is expected to take several months.

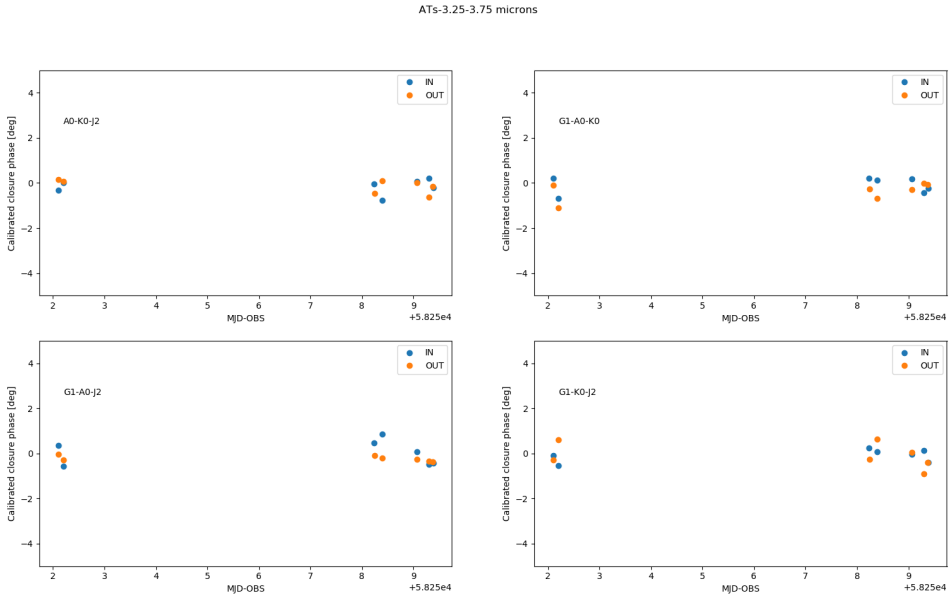

Figure 8: Stability of the calibrated closure phase in L band with ATs. The closure phases have been averaged over the 3.25-3.75 µm range. The observations and baselines are the same as in figure 7. The dispersion of measures is much less sensitive to seeing and to baseline than the absolute visibility and the overall rms is <0.8° for all baseline triplets.

6.6 Absolute visibility accuracy in N band with ATs

In N band with ATs, the selected sources with magnitudes between 15 and 30 Jy in N resulted too faint to produce accurate absolute visibilities and we had to make a new selection of brighter sources, which usually were much poorer calibrators. Figure 9 shows the absolute visibility as a function of time during one good seeing night (although the seeing is not expected to be the dominant parameter for N band accuracy). We find that the rms of the absolute visibility very rapidly increases when the N band flux decreases below typically 30 Jy. Our calibrators in the range 15 to 28 Jy yield a rms of corrected visibility larger than 30% (30% is the specification for 20 Jy measurements) while for target brighter than 29 Jy,

the rms is less than 5%. This results from errors in the photometric calibration. We are still investigating this point and find that the photometry with one beam or telescope (AT1) is much larger than the others. We need further tests to clarify this point. The current conclusion is that, like with MIDI, the limiting flux for a good coherent flux is substantially fainter than this for a correct photometric and hence absolute visibility calibration.

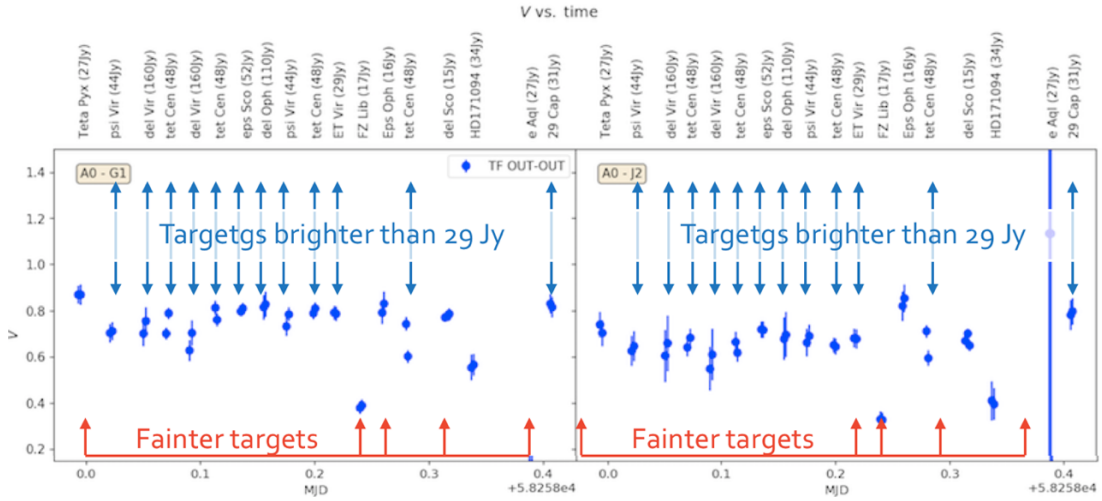

Figure 9: visibility as a function of time for calibrators (corrected from the estimated diameter). For targets brighter than 29 Jy we get a rms of the visibility of 4.8%. For targets between 15 and 27 Jy, the rms of the visibility measures is larger than 30%

6.7 Absolute and differential visibility accuracy in the N band with UTs

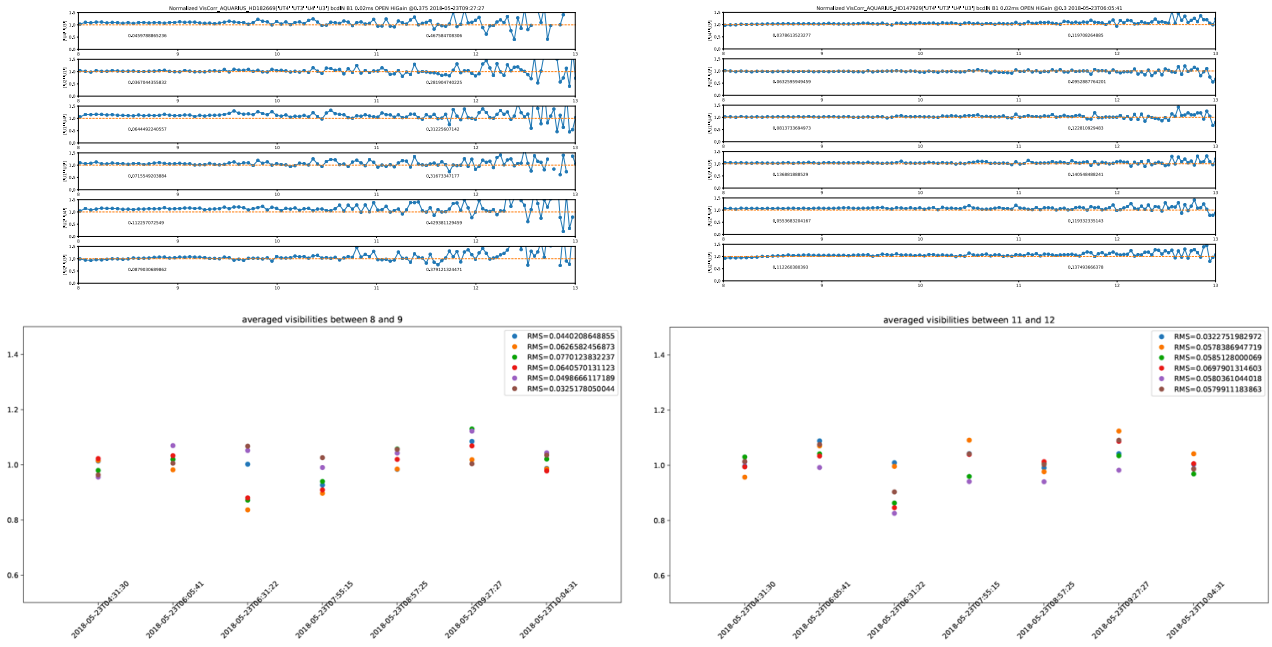

Figure 10: Calibrated absolute visibility in N band with UTs. Upper left HD182669 (N=2.5 Jy) and upper right HD147929 (N=7.5 Jy). Both have been calibrated by the average between HD138492 (N=8 Jy) and HD186765 (N=8.6 Jy). For each baseline, we indicate the rms per spectral channel in the 8-9 μm and the 11-12 μm bands. The lower plots indicate the variation over time and the rms of the average visibility for each baseline (from top to bottom: UT3-4, UT1-2; UT1-4; UT1-3; UT2-4; UT2-3), computed in the 8-9 μm band (lower left) and 11-12 μm band (lower right). This observation represents 7 targets (8 Jy, 7.5 Jy, 3 Jy, 3.1 Jy, 5.5 Jy, 2.5 Jy and 8.6 Jy from left to right) and cover a time span of 6 hours.

So far, we could use only two half nights with 4 UTs for the commissioning of MATISSE and we could therefore not observe a large number of triplets. As our first goal was to evaluate the quality of measures for relatively bright targets we concentrated on stars with magnitudes between 2 and 9 Jy, which should be roughly equivalent to a 40-180 Jy range with ATs. The results are summarized in figure 10. The lower plots show the average absolute visibility computed between 8 and 9 μm (left) and 11 et 12 μm (right), for 7 targets observed over a total interval of 6 hours. The rms of the absolute visibility ranges from ~3.5% to ~7.5% in both band, which is between the 7.5% specification and the 2.5% goal. The upper plots show V(λ) for the full N band for a 2.5 Jy and a 7.5 Jy target, both calibrated by the average between one 8 Jy and one 8.6 Jy target. We have computed the rms in the spectral direction of the absolute visibility by spectral channel in the 8-9 μm and the 11-12 μm bands. For the 8-9 μm band, the visibility rms goes from 3.6 % to 13% for both targets and we are clearly dominated by variations of the instrument + atmosphere visibility. In the 11-12 μm case, the brightest star has a rms range of 9.5% to 14% while the faintest one shows a rms range of 28% to 47%. We compute also the differential visibility $V(\lambda)/\langle V(\lambda)\rangle_\lambda$ with a spectral average $\langle V(\lambda)\rangle_\lambda$ computed for each target and each baseline over the 8-10 μm interval. In the 8-9 μm band, we obtain differential visibility rms ranging from 2% for the shortest baseline to 10% for the longest baseline, almost independently of the target flux in the 2.5 Jy to 8.6 Jy range. In the 11-12 μm band, the differential visibility rms is between 4% and 8% for all baselines for targets brighter than 4 Jy and from 10% to 20% on the targets fainter than 3.2 Jy.

6.8 Calibration of the differential phase in LR

The LR differential phase is critical to detect faint companions and more generally to improve the polychromatic image reconstruction. This should be the most accurate MATISSE measurement if we consider only the contribution of fundamental noise, but the differential phase is strongly sensitive to the chromatic OPD mixed with instrumental effects.

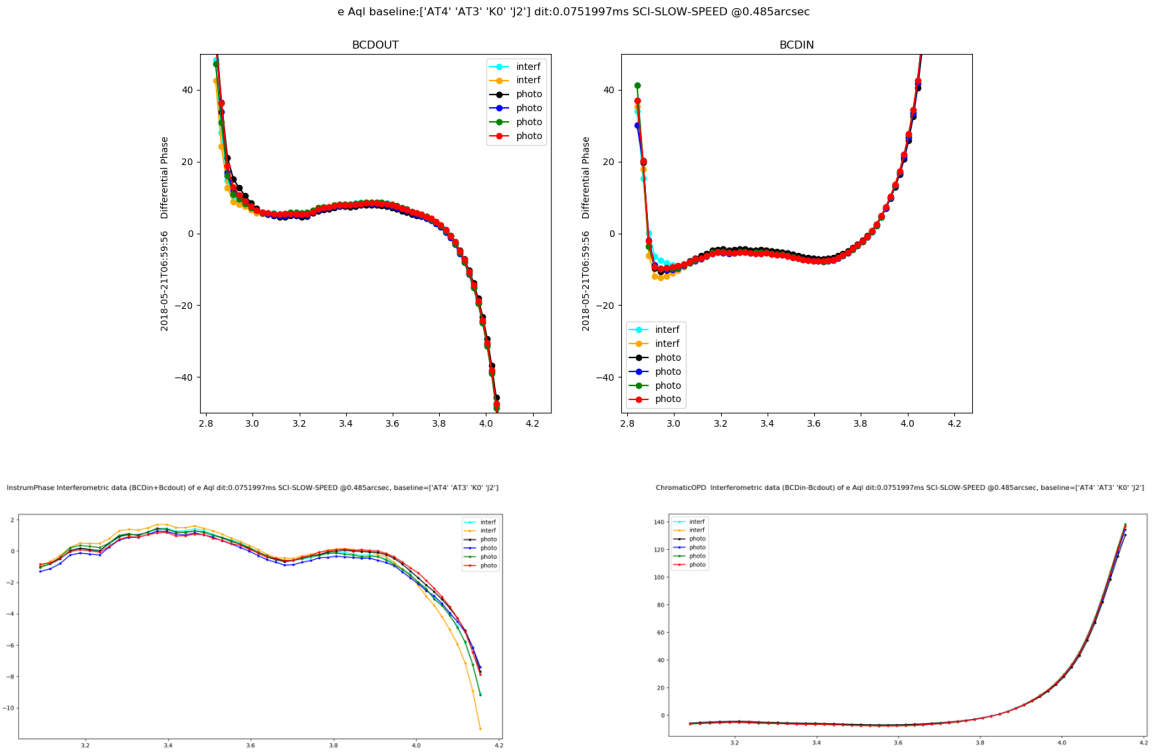

Figure 11: Low Resolution differential phase in the L band on baseline 1. The upper curves show the raw differential phase obtained on a 152±28 Jy calibrator. Here, the DRS has corrected only the achromatic OPD fitted between 3.1 and 3.9 μm. We have 6 exposures with the "BCD out" setup (left) and with the "BCD in" setup (right). The time shift between exposures go from 1 to 10 mn. The BCD inverts the source + atmosphere contribution without changing the instrument contribution. The lower left curve shows the BCD "in+out" differential phase that cancels the source and atmosphere contribution and shows only, in principle, the instrument and detector contribution. The lower right curve shows the BCD "in-out" differential phase that is in principle only the target + atmosphere contribution dominated by the chromatic OPD.

In section 6.3 we have seen that the accuracy of the closure phase is also limited by the contamination by chromatic OPD. A good calibration of this chromatic OPD from the differential phase would also contribute to boost the accuracy of the closure phase and hence the dynamical range of the reconstructed images. To separate the target + atmosphere effects from the instrument effects, we use a Beam Commuting Device (BCD) that inverts beams 1 et 2 and beams 3 and 4 without any change in image position or in OPD inside MATISSE. This changes the sign of the differential phase on baselines 1 and 2 without changing the instrumental response. As the BCD can be commuted in a few seconds between each exposure, the BCD calibration cycle can be as fast as 2 minutes, unlike the calibration with a reference star that will see the instrument changes in 30 mn and merge the chromatic OPD from the two stars. Figure 11 shows the LR differential phase on baseline 1 obtained on a 150 Jy calibrator. The initial differential phase recipe in the DRS corrected both the piston and the chromatic OPD from a model. This failed because it merged the piston estimate with the errors of the chromatic OPD model, which was never tested in L before. Here we have fitted only an achromatic piston between 3.1 and 3.9 µm. The raw differential phases vary by a few degrees in a few minutes and show a strong instrumental contribution below 3 µm, that is not inverted by the BCD and global chromatic OPD, very strongly enhanced near the end of the L band after 3.9 µm that is inverted by the BCD. The BCD "in+out" differential phase shows the instrumental contribution drift over 10 mn that is of the order of 0.5° except after 4 µm where a residual chromatic OPD contamination (through the piston correction) can be suspected. The BCD "in-out" shows the chromatic OPD. The stability of the measure between 3.1 and 3.8 µm is of the order of 0.3° rms per spectral channel, a number that is likely to be improved if we succeed to properly fit the evolution of the chromatic OPD with time. The quality of this fit will set the ultimate accuracy on the LR differential phase.

7. ACCURACY OF MATISSE HR MEASURMENTS IN THE L BAND

The Figure 12 shows the HR L band spectrum of a star with a gas envelope producing hydrogen lines. It reveals the richness of the emission spectrum in the L band and is used for spectral calibration. Unfortunately, the coherence time in L bands and the speed of the Hawaii detector in its high SNR "Slow Read" mode strongly limit the spectral coverage until we can use an external fringe tracker.

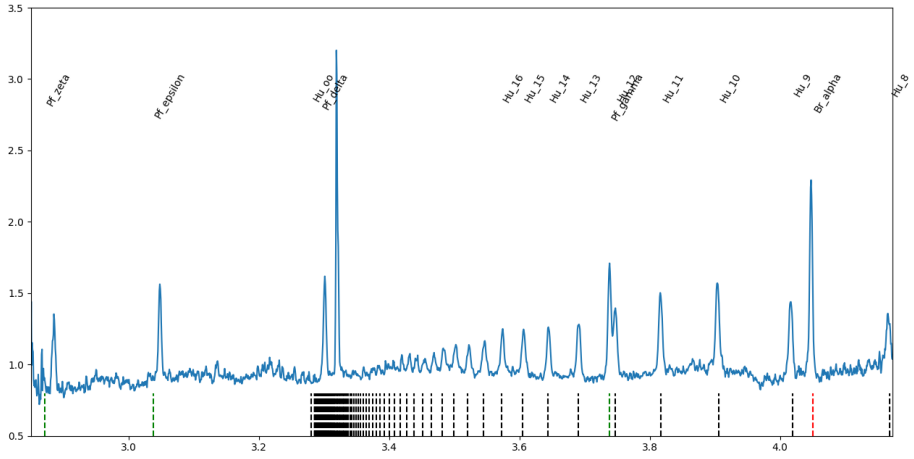

Figure 12: Emission line spectrum of a Be star. The continuum has been flattened. In addition to Brα we see strong Pfund lines and the end of the Humphrey series.

The figure 13 shows the spectrum, the differential visibility and the differential phase obtained in the L band high spectral resolution (HR=920) on a typical Be star with a gas rotating disk. The spectral coverage is limited to a small window of typically 0.1 µm for a DIT=111 ms. The user has to define the central wavelength and to select one of the proposed DITs and the window width is automatically adapted. Here the window has been centered on the Brα emission line. For this 20 Jy target, the differential phase accuracy ranges from 0.3° to 1° and the differential visibility accuracy range from 1.5% to 4% per spectral channel and per 1 mn exposure. These numbers will probably improve when we improve the fit of the chromatic OPD that bends the continuum in the two differential measures.

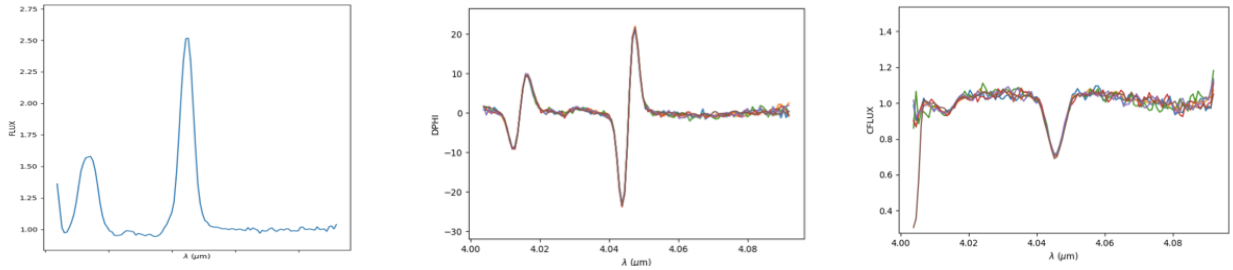

Figure 13: spectrum (left), differential phase (center) and differential visibility (right) for L band HR observations with UTs of a Be star with a rotating gas envelope producing emission lines (here Brα).

8. CONCLUSION

Four months after the beginning of its commissioning, MATISSE is fully operational in its Hybrid mode and in all spectral resolutions, but the Very High Spectral Resolution in L and M. It can be operated as any VLTI instrument. The specific feature used by MATISSE is the chopping, which works fine with ATs but could not be tested at frequency higher than 0.5 Hz with UTs. The data processing and pipeline of MATISSE are operational and all results shown in this paper have been obtained from data processed by the pipeline. Additional tools in Python have been used only for plots and statistics. The table 2 below summarizes the results presented in this paper.

Name	Tech Specs specific.	Tech Specs Goal	Commissioning preliminary values
Sensitivity in L UT (4T, LR)	≤ 0.75 Jy	≤ 0.15Jy	<0.1 Jy (extrapolation)
Sensitivity in L AT (4T, LR)	≤ 7.5 Jy	≤ 1.5Jy	0.2 Jy achieved
Sensitivity in N UT (4T, LR)	≤ 4 Jy	≤ 1 Jy	0.21 Jy achieved
Sensitivity in N AT (4T, LR)	≤ 60 Jy	≤ 12.5Jy	~10 Jy estimated from coherent flux SNR
Visibility accuracy L UT	≤ 7.5%	≤ 2.5%	TBI, should be ≤ than with ATs
Visibility accuracy L AT	≤ 7.5%	≤ 2.5%	<8% including diameter errors, 1% if good seeing and no diameter errors (short baselines)
Visibility accuracy N UT	≤ 7.5%	≤ 2.5%	U_{12}:6.2%; U_{13}:6.4%; U_{14}:7.7%; U_{23}:3.2%; U_{24}:5%; U_{34}:4.4% over 6 hours.
Visibility accuracy N AT	≤ 30%	≤ 10%	<5% if N>30 Jy; ≥30% in the 15-27 Jy range
Diff. phase accuracy L UT	≤ 30 mrad	1mrad	<1° (17 mrad) for HR
Diff. phase accuracy L AT	≤ 60 mrad		<1° if we control the chromatic OPD
Diff. phase accuracy N UT	≤ 30 mrad	1mrad	TBI
Diff. phase accuracy N AT	≤ 60 mrad		TBI
Closure phase accuracy L UT	≤ 40 mrad	1mrad	TBI
Closure phase accuracy L AT	≤ 80 mrad		0.8° (14 mrad) rms broad band, 2° PTV broad features
Closure phase accuracy N UT	≤ 40 mrad	1mrad	1.5° (26 mrad) PTV spectral features, 0.2° rms at 30 Jy
Closure phase accuracy N AT	≤ 80 mrad		Global 10° at 30 Jy, H Sco (30 Jy) <5°
Diff visibility accuracy L UT	≤ 1.5%	≤ 0.5%	1.5% HR in the center. Needs better fit in the continuum.
Diff visibility accuracy N UT	≤ 3%	≤ 1%	2% to 10% instrumental features
Diff visibility accuracy L AT	≤ 5%	≤ 2%	TBI
Diff visibility accuracy N AT	≤ 30%	≤ 10%	TBI

Table 2: summary of the MATISSE specifications and goals that have been tackled in this paper. "Green" means that we are within specifications. "Orange" means that we are close to the limit but likely to improve thinks with a better processing and calibration.

- The acquisition limits are well below the best goals. This also indicates that the SNR on the coherent flux is good for fainter sources than expected.
- The closure phase is within specifications in L with ATs and in N with UTs. In N with ATs the situation is unclear and we have to investigate more the magnitude limit that allows to have a closure phase good enough for imaging.
- The absolute visibility accuracy in L should be within specifications in good nights or if we choose carefully the frame exposure time. In N, we have accurate absolute visibilities for bright targets but seem to hit an accuracy

limit below 30 Jy with ATs. In the July run we will test new background correction procedures using a slit instead of a pinhole.

- The differential phase is within specifications but very far from the goals. The main problem, mainly at low spectral resolution, is to model or at least follow correctly the evolution of the atmospheric chromatic OPD.
- The differential visibility is acceptable for the best baselines but quite out of specifications for the worst ones. This is probably due to detector features and might be improved by better detector cosmetics.

Finally, there is quite a lot of measures that still need to be investigated (TBI) from existing data.
Overall, the results are very encouraging but we have to be careful as quite a few estimates are still based on very few data.

ACKNOWLEDGEMENTS

We have a great debt toward Mr. Fabio Rojas, an agent of the "office for foreigners" of the Chilean PDI, who made a decisive contribution to the success of the MATISSE commissioning by easing a cumbersome residence permit issue.
We have restricted the list of co-authors of this paper to the people that have actively participated to the commissioning runs and data reduction. We are extremely grateful to the full MATISSE consortium, who allowed MATISSE to be designed, funded, built and integrated, and to the ESO staff at Paranal and Garching who supported the project and its installation on the VLTI. A broader list of MATISSE consortium members and supporters can be found in the references [2] and [3].

REFERENCES

[1] Woilez, J., et al, "VLTI status update: three years into the 2nd generation", Proc. SPIE 10701, (2018).
[2] Lopez, B., et al, "An Overview of the MATISSE Instrument — Science, Concept and Current Status," The Messenger, 157, 5-12 (2014).
[3] Lopez, B., et al, "The MATISSE instrument at the VLTI," Proc. SPIE 10701, (2018).
[4] Robbe-Dubois, S., et al, "MATISSE: Performance in laboratory, results of AIV in Paranal, and first results on sky," Proc. SPIE 10701, (2018).
[5] Chelli, A., et al, "Pseudomagnitudes and differential surface brightness: Application to the apparent diameter of stars," Astronomy & Astrophysics, 589, (2014).
[6] Mathar, R. J., "Refractive index of humid air in the infrared: model fits," Journal of Optics A: Pure and Applied Optics, 9(5), 470-476 (2007).